Effective Diffusion-Medium Thickness for Simplified Polymer-Electrolyte-Fuel-Cell Modeling

Adam Z. Weber*

Lawrence Berkeley National Laboratory,
1 cyclotron road, MS 70-108B, Berkeley, California 94720, USA

In this manuscript, conformal mapping is applied to a rib/channel domain of a polymer-electrolyte-fuel-cell diffusion medium. The analysis leads to the calculation of an effective diffusion-medium thickness, which can subsequently be used in 1-D simulations to account for the average rib/channel 2-D geometric effect. Extensions of the analysis to anisotropic and multilayer diffusion media are also given. Both equations and figures show the impact on a given variable at the catalyst layer of having a combined conducting/nonconducting boundary across from it.

Keywords: Polymer-electrolyte fuel cell; mathematical modeling; conformal mapping; gas-diffusion layer; diffusion medium

* Corresponding author: azweber@lbl.gov, 510-486-6308

1. Introduction

Mathematical modeling has been shown to provide understanding of the complex operation of polymer-electrolyte fuel cells (PEFCs) [1, 2]. Modeling has the ability to sort out and quantify the various tradeoffs and interplay among the different PEFC phenomena. Key among these is the impact of thermal and water management in the PEFC backing layers know as diffusion media (DM). A DM is typically composed of a macroporous gas-diffusion layer (GDL) and a microporous layer (MPL). In addition, each layer contains mixed wettability composed of hydrophilic (carbon) and hydrophobic (Teflon) moieties to aid in water egress and reactant-gas ingress. The transport in these layers is often compounded by the fact that while one end is in contact with the catalyst layer, the other end is typically in contact with a solid portion or rib and an open portion or channel. The rib allows for electrical and better thermal connections and the channel allows for water and gas connections.

It is widely known that as one adds complexity to a model, computational cost increases and model robustness decreases. This is one reason why many of the detailed models for PEFCs and their constitutive layers are often 1-D or pseudo 2-D where the flow-channel direction is also considered. In this fashion, the 2-D rib/channel geometry is neglected. Accounting for such geometry and its effects normally requires simplification of the governing equations [3-9]. In this article, such simplification is not used and the average effects of the rib/channel geometry is accounted for in a 1-D simulation by the use of an effective DM thickness that is derived from integrating a semianalytic series solution.

To undertake such a task, conformal mapping is used to predict how the average value of a flux changes as a function of the rib-to-channel ratio. This change is then correlated to an effective DM thickness for a 1-D simulation that accounts only for transport in the through-plane

direction. The effective thickness is similar to making the DM thicker to result in the larger mass-transport resistances due to having a boundary that is not only conducting but nonconducting as well. Thus, the average 2-D impact of the rib/channel geometry can be assessed and utilized without increasing the complexity and dimensionality of a 1-D simulation. It should be noted that such an analysis provides only the average impact and not the detailed distribution with maxima and minima; to capture these detailed effects requires a full 2-D simulation.

2. Problem Statement and Conformal Mapping

The problem statement and conformal-mapping solution method for the DM is summarized schematically in Figure 1. Figure 1a shows a PEFC with the domain under investigation highlighted. The left figure in Figure 1b shows the rib/channel geometry where t is the thickness of the DM, L is the length of the modeling domain (combined rib and channel half lengths), δ represents the dimensionless location of the rib/channel interface, and $y = 0$ is the middle of the DM (*i.e.*, the catalyst layer is at $t/2$). The hatched portion represents the channel where gas and liquid can interchange (for a variable like electronic potential, the boundary conditions on **AE** and **ED** are switched). The top and bottom boundary conditions are due to symmetry.

A quasipotential solution method can be used assuming that the overall fluxes within the domain are uniform, which is the case in a DM if one assumes local equilibrium between liquid water and water vapor if both are present. One can then define a variable, Q, the quasipotential, which is related to the divergence of a flux [10-14]

$$N = \nabla Q \tag{1}$$

The flux can be any flux in the domain and often the current density or reactant-gas flux is chosen. The actual transport equation for the given flux is irrelevant for this analysis as long as it is first order. Hence, nonlinear equations can be used. The above two conditions result in Laplace's equation within the domain

$$\nabla^2 Q = 0 \tag{2}$$

If the two conditions are not met, full 2-D finite-element or similar computational-fluid-dynamics simulations are required and the analysis presented in this article is not rigorously valid. In terms of the boundary conditions, at the gas channel the variables are set to known values, Q is set equal to zero, and at the catalyst layer, the flux is set (*e.g.*, from a Butler-Volmer kinetic equation).

As shown in Figure 1, conformal mapping is used to switch from the real domain to a domain in which the problem becomes 1-D. The overall procedure is to use Schwartz-Christoffel transformations to transform the initial geometry in the z-plane to the upper half of the w-plane and then into a rectangle in the a-plane [15, 16]. The transform from the w-plane to the z-plane is given by

$$z = C\int_0^w \frac{dw}{\sqrt{w-a}\sqrt{w-b}\sqrt{w-c}\sqrt{w-d}} \tag{3}$$

where the lower case letters correspond to the location of the z-plane vertices in the w-plane. This transformation can be rewritten and manipulated to be of the form [14, 17]

$$z = \frac{t}{2K(k)} F(w;k) \tag{4}$$

where $F(w;k)$ and $K(k)$ are the incomplete and complete elliptical integrals of the first kind, respectively [18], and $k = c^{-1}$ and can be determined from the transcendental equation

$$\frac{2L}{t} = \frac{K\left(\sqrt{1-k^2}\right)}{K(k)} \tag{5}$$

The above transform can be inverted to yield the transform from the *z*-plane to the *w*-plane [17, 18]

$$w = \mathrm{sn}\left(\frac{2K(k)}{t} z, k\right) \tag{6}$$

where sn is an elliptic function (which is tabulated in handbooks [18, 19]), and expressions for *u* and *v* can easily be obtained by known elliptic-function identities [17-19]. Now, all of the points in *w*-plane have been determined. Specifically,

$$a = -b = -1;\ \ d = -c = -\frac{1}{k};\ \ e = -\frac{\mathrm{dn}\left(\frac{2K(k)}{t}\delta L, \sqrt{1-k^2}\right)}{1-k'^2\,\mathrm{sn}^2\left(\frac{2K(k)}{t}\delta L, \sqrt{1-k^2}\right)} \tag{7}$$

where dn is also an elliptic function.

Next, one must transform the *w*-plane into the *a*-plane. The resulting Schwartz-Christoffel transformation is

$$a = -\int_{-1}^{w} \frac{dw}{\sqrt{w-1}\sqrt{w+1}\sqrt{w-c}\sqrt{w-e}} \tag{8}$$

where this integral has to be evaluated numerically.

The boundary conditions must be transformed. Since insulators remain insulators and Dirichlet boundary conditions remain intact through the transformations, only the flux boundary-

condition at the catalyst layer, $N(Q)$, has to be transformed. This transformation is done by examining the respective transformations along **BC** in Figure 1, with the result [14],

$$G(Q,a_i)=\frac{t}{2kK(k)}N(Q)\frac{\sqrt{u-e}}{\sqrt{u+c}} \tag{9}$$

2. Comparison of Solutions and Effective Thickness

For a typical 1-D problem, the rib (**ED** in Figure 1) is neglected, resulting in case similar to that of the right figure in Figure 1, except in the original coordinate system. Solving for the variable Q (related to the divergence of the flux) in the typical 1-D problem results in

$$Q=Q_0+N\left(x+\frac{t}{2}\right) \tag{10}$$

For the transformed system, a similar solution exists if one only cares about the average value of the flux, $\overline{G}$, which is essentially taking the first eigenvalue of the series solution for Q. Doing the averaging and solving for Q in the a-plane of Figure 1 results in

$$Q=Q_0+\frac{Nt}{2kK(k)}\frac{\int_0^{a_c}\frac{\sqrt{u-e}}{\sqrt{u+c}}da_i}{a_{\mathbf{C}}}a_r \tag{11}$$

To determine the effective thickness of the DM caused by having the rib/channel geometry, the variable value at the catalyst layer in the a-plane (*i.e.*, at $a_{\mathbf{B}}$) is determined, and the thickness of the 1-D problem modified to result in the same value of Q. These manipulations result in

$$Q-Q_0=\frac{Nta_{\mathbf{B}}}{2kK(k)}\frac{\int_0^{a_c}\frac{\sqrt{u-e}}{\sqrt{u+c}}da_i}{a_{\mathbf{C}}}=Nt_{\text{eff}} \tag{12}$$

and so, the effective thickness can be written as

$$\frac{t_{\text{eff}}}{t} = \frac{a_{\mathbf{B}}}{2kK(k)} \frac{\int_0^{a_{\mathbf{C}}} \frac{\sqrt{u+c}}{\sqrt{u-e}} da_i}{a_{\mathbf{C}}} \tag{13}$$

Before examining the results, a comment should be made regarding the case of when the insulating boundary is the channel and not the rib (*i.e.*, **AE** not **ED**), such as in the case for the electrical potential. For this case, the transformation from the *z*-plane to the *w*-plane is the same (see equations 4 and 6), but a different transform is required from the *w*-plane to a different *a*-plane, noted as the a_Φ-plane, since the conducting boundary is different. This transformation is given by

$$a_\Phi = -\int_e^w \frac{dw}{\sqrt{w+c}\sqrt{w-1}\sqrt{w-c}\sqrt{w-e}} \tag{14}$$

instead of equation 8. This results in an effective-thickness expression of

$$\frac{t_{\Phi\,\text{eff}}}{t} = \frac{a_{\Phi\mathbf{B}}}{2kK(k)} \frac{\int_0^{a_{\Phi\mathbf{C}}} \frac{\sqrt{u+1}}{\sqrt{u-e}} da_{\Phi i}}{a_{\Phi\mathbf{C}}} \tag{15}$$

The two effective-thickness equations can be solved and are plotted in Figure 2. The integrals are evaluated using a 25-term Gauss-Legendre integration method where the a_i's are specified and the corresponding *u* values calculated using an implicit equation solver along with the *a*-plane transformations (equations 8 and 14) [19]. Once again, the effective thickness can be seen as how much thicker the DM has to be in order to contain the same mass-transport resistance when part of the boundary is nonconducting. As expected, the two curves are symmetric with respect to the rib/channel interface due to the geometry of the initial problem;

they cross at a rib-to-channel ratio of 1. The curves approach values of 1 and infinity as the insulating and conducting boundary vanishes, respectively. Depending on if flow through the rib or the channel is limiting (based on looking at relative transport coefficients and their effects), one can quickly determine in what range the optimum rib-to-channel ratio lies; however, such an analysis is beyond the scope of this paper. Figure 2 and equations 13 and 15 can be used in 1-D or 2-D simulations where the flow-channel direction is considered to account for the rib/channel geometry in an average sense. For ease of analysis and use, the Q curve in Figure 2 has been fit to an exponential expression

$$\frac{t_{\text{eff}}}{t} = 0.94 + 5.42\exp(-4.21\delta) + 5.95\exp(-32.6\delta) \tag{16}$$

For the Q_Φ curve, one needs only replace the δ above with $1-\delta$. It should be noted that while the above expression fits the curve well, it does not capture adequately the steep increase towards infinity as δ goes to 0, and so should be used with caution in the limits of small conducting or nonconducting regions.

3. Model Extensions

It is worthwhile to examine two additional issues that are relevant for determining effective thicknesses, namely, multilayer DM and anisotropic DM. Both are addressed below. It should be noted that the analysis presented below is not strictly rigorous because the existence of multiple layers and anisotropic properties causes geometry-dependent equations, which limits the use of the quasipotential transformation method. This limitation arises because the geometric dependence cannot be canceled entirely [14]. The conformal mapping remains valid and for a single equation there should be minimal error. The amount of error depends on various factors

including geometry, material and physical properties, operating conditions, etc. The error and that of using a 1-D model instead of a full 2-D will increase with the number of layers (*i.e.*, there are more interfaces that are averaged over) and number of equations. Quantification of the error for various PEFC test cases is currently under investigation.

In terms of multilayer DM, because the governing equations are the same as those of a single-layer DM (only the properties change), the above analysis remains valid. Therefore, equations 13 and 15 can be used. However, those equations yield the change in the total thickness of the composite DM. It can be shown that in terms of the average thickness values, the relative location of the MPL remains the same in both the *z*- and *a*-planes [14]. Hence, the effective thickness of the GDL and MPL in a composite DM can be given by

$$t_{\mathrm{eff,GDL}} = \frac{t_{\mathrm{eff}}}{t}\left(t - t_{\mathrm{MPL}}\right) \tag{17}$$

and

$$t_{\mathrm{eff,MPL}} = t_{\mathrm{eff}} - t_{\mathrm{eff,GDL}} \tag{18}$$

respectively, where t remains the total thickness of the composite DM.

For anisotropic DM one can stretch the 2-D domain into an equivalent one that is isotropic. As an example, if one assumes that the flux relation can be written in the form of a conduction equation (*e.g.*, Fourier's law for heat conduction, Darcy's law for fluid flow, Ohm's law for current flow), then the governing equation is

$$\alpha_x \frac{\partial^2 Q}{\partial x^2} + \alpha_y \frac{\partial^2 Q}{\partial y^2} = 0 \tag{19}$$

For the equivalent, isotropic domain, the through-plane or x-dimension is kept the same (*i.e.*, $(\partial x)_e = \partial x$) and the y-dimension is stretched by $(\partial y)_e = \sqrt{\alpha_x / \alpha_y}\,\partial y$. Doing this substitution results in

$$\alpha_x \frac{\partial^2 Q}{(\partial x)_e^2} + \alpha_x \frac{\partial^2 Q}{(\partial y)_e^2} = 0 = \nabla_e^2 Q \tag{20}$$

The equivalent domain can then be used in the conformal mapping to yield the effective DM thickness as per equations 13 and 15. Thus, the only change would be that the domain length, L, would be replaced by an effective length,

$$L_{\text{eff}} = L\left(\frac{\alpha_x}{\alpha_y}\right)^{\frac{1}{2}} \tag{21}$$

before proceeding with the analysis. This effective length impacts the solution in the previous section since a different value of k (see equation 5) would be calculated. If one does not have flux relations in the form of a conduction equation, a similar analysis can also be used to determine the correct equivalent-system geometry [20]; such a discussion is beyond the scope of this article. In addition, because 1-D or average solutions are desired, it should be possible to perform different coordinate transformations and equivalent domains depending on the various property anisotropies; this is currently being investigated and validated.

Figure 3 displays several curves for the inverse effective thickness and the case where the channel is conducting as a function of transport-coefficient anisotropy; the curves for a rib-conducting boundary are symmetric. The inverse thickness is plotted because it ranges from 0 to 1 and thus allows a better comparison as to the limiting behavior as the conducting boundary approaches zero thickness (*i.e.*, the effective thickness goes towards infinity). The chosen value

for the isotropic situation is arbitrary for this comparison since one is only changing the value of L in equation 5, and it is the same curve as that of Q in Figure 2. From Figure 3, as well as by inspection of equation 21, one can see that as α_y increases compared to α_x, the effective length becomes shorter and the impact of the rib/channel geometry less. This agrees with more rigorous simulations that show a more uniform profile as the in-plane conductivity increases compared to the through-plane one [21], which is typically the case for PEFC DM due to the carbon fiber orientation of the material.

Figure 3 suggests that there is a limitation that occurs when α_y is appreciably smaller than α_x. This limit makes sense since as the through-plane conductivity dominates, there is no in-plane spreading out of the variable. Thus, conduction of the component occurs in a straight path from the conducting boundary to the catalyst layer, with the part of the catalyst layer across from the nonconducting boundary being inactive. The limiting curve is essentially a measure of the maximum loss of catalyst-layer utilization. In this fashion, Figure 3 can be used not only to examine the impact of anisotropies, but also the impacts of absolute rib and channel lengths.

5. Conclusions

In this manuscript, conformal mapping has been used to show how the average value of the flux through a diffusion medium (DM) changes as a function of the rib-to-channel ratio. This change allows the calculation of an effective DM thickness that can be used in 1-D simulations and still consider the rib/channel effect. The analysis showed the impact of the rib/channel geometry and can be used as an initial screening for optimal rib/channel ratios. Extensions of the analysis to anisotropic and multilayer DM were also given, with results showing how anisotropies can either yield large inactive zones or a decrease in the rib/channel effect; the latter

is the expected outcome for typical DM materials. The analysis presented is valid for any flow-field design that has a solid and channel portion and it provides the general impact without having to do full 2-D simulations.

Acknowledgements

This work was supported by the Assistant Secretary for Energy Efficiency and Renewable Energy, Office of Hydrogen, Fuel Cell, and Infrastructure Technologies, of the U. S. Department of Energy under contract number DE-AC02-05CH11231 and industrial sponsors.

List of Symbols

Roman

a	transformed plane where geometric problem is solved
a	point **A** in w-plane, value is taken to be –1
a_Φ	transformed plane where geometric problem for the electronic potential is solved
a_i	imaginary-axis direction in the a-plane, cm
a_r	real-axis direction in the a-plane, cm
$a_{\Phi i}$	imaginary-axis direction in the a_Φ-plane, cm
$a_{\Phi r}$	real-axis direction in the a_Φ-plane, cm
b	point **B** in w-plane, value is taken to be 1
c	point **C** in the w-plane
d	point **D** in the w-plane
dn(x)	elliptic function dn of argument x
e	point **E** in the w-plane
G	transformed oxygen flux boundary condition, mol/cm^{2}s
k	defined as 1/c
K(x)	incomplete elliptic integral of the first kind or argument x
L	diffusion medium width, cm
L_{eff}	effective diffusion medium width for equivalent geometry, cm
N	superficial flux density of oxygen, mol/cm^{2}s
Q	quasipotential
Q_Φ	electronic current quasipotential
sn(x)	elliptic function sn of argument x

t diffusion medium or layer thickness, cm

t_{eff} effective diffusion medium or layer thickness for 1-D simulations, cm

u real-axis direction in the w-plane, cm

v imaginary-axis direction in the w-plane, cm

w Schwartz-Christoffel transformed plane

x through-plane (DM) or real-axis direction in the z-plane, cm

y channel or imaginary-axis direction in the z-plane, cm

z along-the-channel direction in the z-plane, cm

Greek

α generic transport coefficient

δ dimensionless channel length

Subscripts/Superscripts

B location of **B** in the respective plane

BC catalyst-layer / diffusion-medium interface

C location of **C** in the respective plane

e equivalent geometry

GDL gas-diffusion layer

MPL microporous layer

References

[1] A.Z. Weber, R. Balliet, H.P. Gunterman, J. Newman, in: M. Schlesinger (Ed.), Modern Aspects of Electrochemistry, vol. 43, Springer, New York, 2008.

[2] A.Z. Weber, J. Newman, Chemical Reviews, 104 (2004) 4679.

[3] C.Y. Wang, Chemical Reviews, 104 (2004) 4727.

[4] A.C. West, T.F. Fuller, J. Appl. Electrochem., 26 (1996) 557.

[5] R. Bradean, K. Promislow, B. Wetton, Numerical Heat Transfer Part a-Applications, 42 (2002) 121.

[6] A.A. Kulikovsky, J. Divisek, A.A. Kornyshev, J. Electrochem. Soc., 146 (1999) 3981.

[7] D. Natarajan, T.V. Nguyen, J. Electrochem. Soc., 148 (2001) A1324.

[8] Z.H. Wang, C.Y. Wang, K.S. Chen, J. Power Sources, 94 (2001) 40.

[9] A. Kazim, H.T. Liu, P. Forges, J. Appl. Electrochem., 29 (1999) 1409.

[10] J.P. Meyers, R.D. Villwock, R.M. Darling, J. Newman, in: J.W. Van Zee, T.F. Fuller, P.C. Foller, F. Hine (Eds.), Advances in Mathematical Modeling and Simulation of Electrochemical Processes and Oxygen Depolarized Cathodes and Activated Cathodes for Chlor-Alkali Processes, The Electrcohemical Society Proceedings Series, Pennington, NJ, 1998.

[11] M.W. Verbrugge, D.R. Baker, J. Newman, J. Electrochem. Soc., 140 (1993) 2530.

[12] D.R. Baker, Siam Journal on Applied Mathematics, 53 (1993) 419.

[13] B. Pillay, J. Newman, J. Electrochem. Soc., 140 (1993) 414.

[14] A.Z. Weber, J. Newman, Siam Journal on Applied Mathematics (2008) submitted.

[15] F.B. Hildebrand, Advanced Calculus for Applications, 2nd Ed., Prentice-Hall, Englewood Cliffs, NJ, 1976.

[16] I.M. Blankson, Journal of Electrostatics, 16 (1984) 33.

[17] N.I. Akhiezer, Elements of the Theory of Elliptic Functions, American Mathematical Society, Providence, RI, 1990.

[18] D. Zwillinger (Ed.), CRC Mathematical Tables and Formulae, 31st Ed., CRC Press, Inc., Boca Raton, FL, 2003.

[19] W.H. Press, S.A. Teukolsky, W.T. Vetterling, B.P. Flannery, Numerical Recipes in Fortran 77, 2nd Ed., Cambridge University Press, Cambridge, 1992.

[20] J. Bear, Dynamics of Fluids in Porous Media, Dover Publications, Inc., New York, 1988.

[21] U. Pasaogullari, P.P. Mukherjee, C.Y. Wang, K.S. Chen, J. Electrochem. Soc., 154 (2007) B823.

Captions

Figure 1. (a) Polymer-electrolyte-fuel-cell schematic with the region of interest highlighted (cathode diffusion medium) which has boundaries of the catalyst layer and a rib/channel where the electrons flow through the rib and the gas and liquid flow through the channel. (b) Simplified schematic of the problem statement for a gas species showing the solution method using conformal mapping; the given boundary points correspond to the known dimensions in the *z*-plane.

Figure 2. Plot of the DM effective thickness for a 1-D simulation as a function of the dimensionless channel length. Shown are curves for both a channel (Q) and rib (Q_{Φ}) conducting boundary.

Figure 3. Plot of the inverse effective DM thickness for a channel conducting boundary as a function of the dimensionless channel length and for various anisotropic transport-property ratios.

(a)

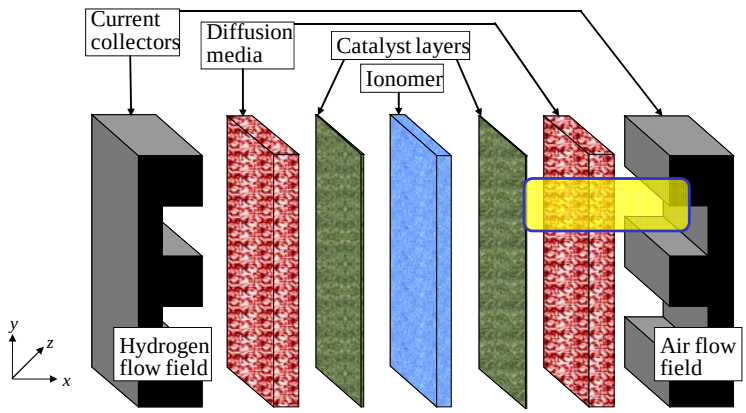

(b)

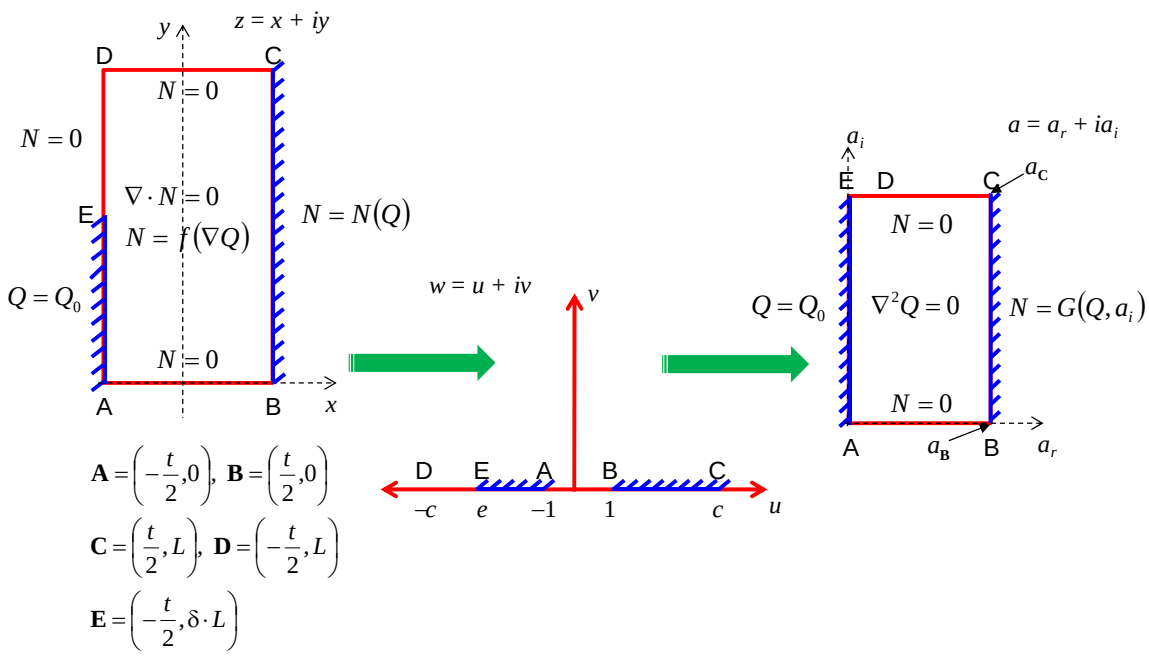

Figure 1. (a) Polymer-electrolyte-fuel-cell schematic with the region of interest highlighted (cathode diffusion medium) which has boundaries of the catalyst layer and a rib/channel where the electrons flow through the rib and the gas and liquid flow through the channel. (b) Simplified schematic of the problem statement for a gas species showing the solution method using conformal mapping; the given boundary points correspond to the known dimensions in the z-plane.

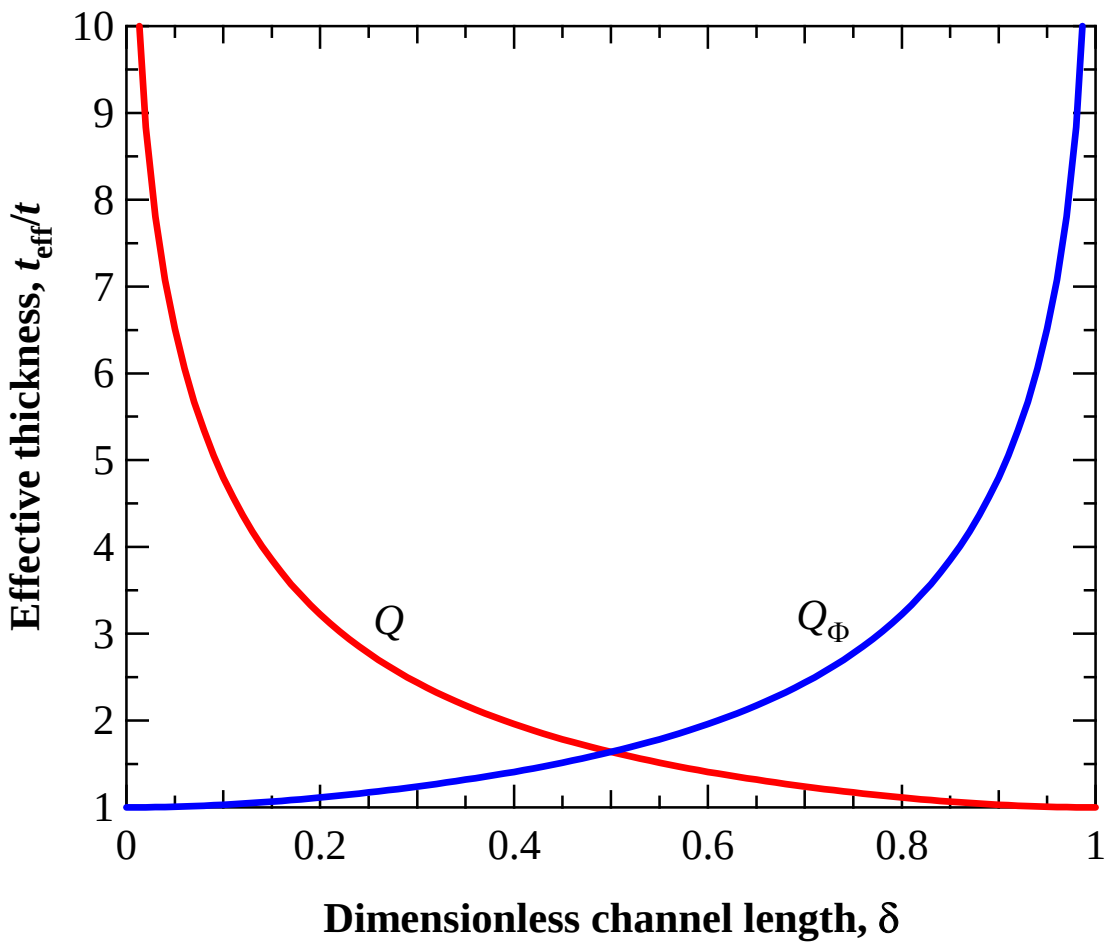

Figure 2. Plot of the DM effective thickness for a 1-D simulation as a function of the dimensionless channel length. Shown are curves for both a channel (Q) and rib (Q_Φ) conducting boundary.

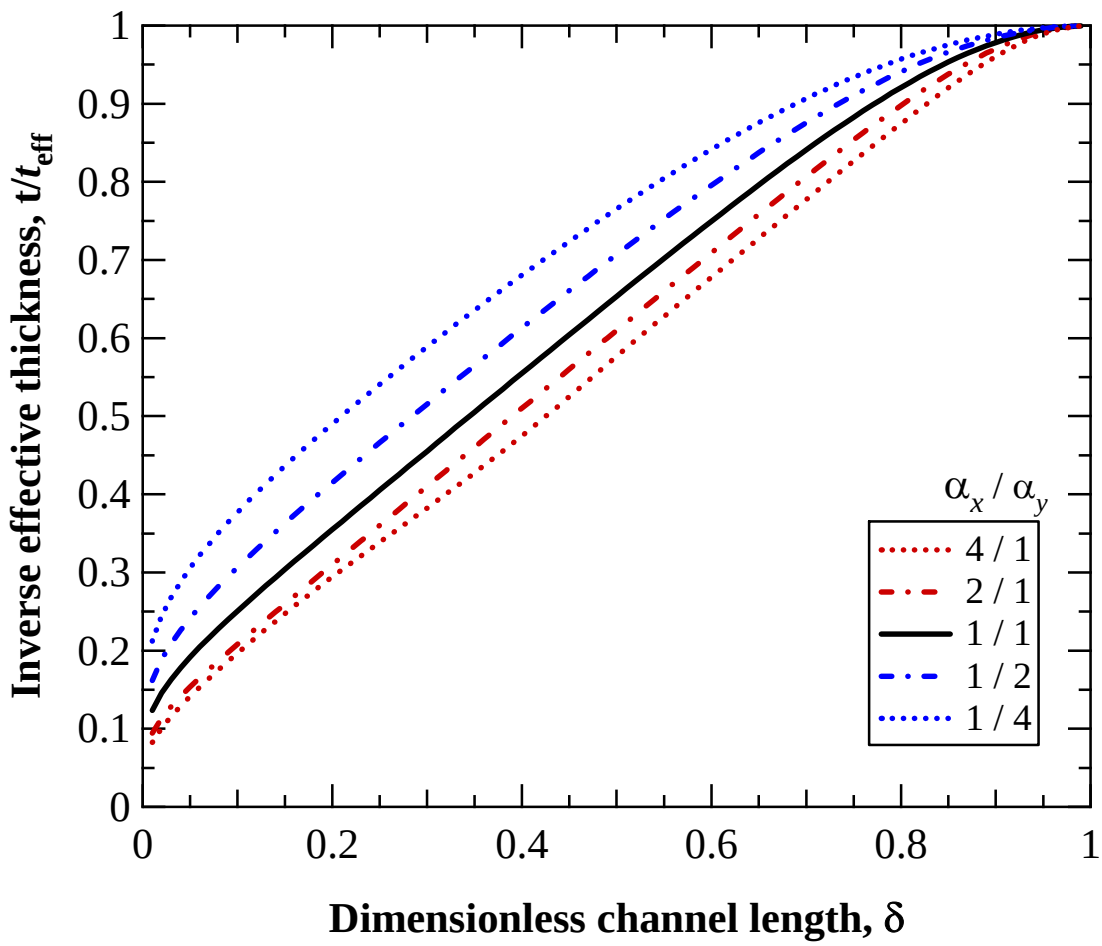

Figure 3. Plot of the inverse effective DM thickness for a channel conducting boundary as a function of the dimensionless channel length and for various anisotropic transport-property ratios.